JEE Journal of Ecological Engineering

Journal of Ecological Engineering, 2026, 27(5), 351–368
https://doi.org/10.12911/22998993/216434
ISSN 2299–8993, License CC-BY 4.0

Received: 2025.12.23
Accepted: 2026.03.16
Published: 2026.04.01

Adsorptive removal of Basic Red 46 by raw corn cob: Optimization using response surface methodology, kinetic modeling, and thermodynamic analysis

Cristian David Gallego Gallo[1*], Natalia Calvo Cardona[1], Nathaly Presiga Posada[1], Angelly Zharick Guarin Pava[1], Angelina Hormaza Anaguano[2]

[1] Research Group on Synthesis, Reactivity and Transformation of Organic Compounds – SIRYTCOR, Faculty of Mines, Universidad Nacional de Colombia, Medellín, Colombia
[2] Research Group on Synthesis, Reactivity and Transformation of Organic Compounds – SIRYTCOR, Department of Chemistry, Faculty of Science, Universidad Nacional de Colombia, Medellín, Colombia
* Corresponding author's email: crgallegog@unal.edu.co

ABSTRACT

Dye-bearing water represents a serious and current drawback that concerns the entire society. An efficient and growing alternative for its treatment is the use of unconventional adsorbents. This work evaluated the adsorption of basic red 46 dye (BR46) onto raw corn cob (CC) using statistical tools. Particularly, a 2^3 factorial design, a steepest ascent approach and an orthogonal central composite surface design were performed, obtaining an optimized process and the interaction between its factors. A removal of 98.1% under a dosage of 5.5 g L^{-1}, initial BR46 concentration of 16.6 mg L^{-1} and contact time of 201.9 min was achieved. The assessment of the equilibrium and kinetics of the BR46-CC system showed the best fit with pseudo-second-order kinetics with $R^2 = 0.94$, while for equilibrium, a better fit was observed with the Redlich-Peterson isotherm, with $R^2 = 0.99$. Thermodynamic parameters proved a spontaneous and exothermic process, with an average Gibbs free energy of -10.0 kJ mol^{-1} and enthalpy of -27.2 kJ mol^{-1}. The entropy of -54.7 J mol^{-1} K^{-1} suggests a reduction in the vibrational capacity of the molecules involved in the process. Furthermore, chemical oxygen demand was evaluated to verify the improvement in water quality after the adsorption process, obtaining a 29% reduction in organic load. These findings highlight the potential of corn cob as a promissory and non-conventional adsorbent for environmental remediation of dye-contaminated water bodies.

Keywords: adsorption, dye-bearing effluents, narrowing path, statistical design, chemical oxygen demand.

INTRODUCTION

Dye-bearing water produced in different economic activities such as textile, food, pharmaceutical, and paint industries, is dumped into natural water resources without prior treatment, compromising the habitat both externally and functionally, since life and several processes that take place there are affected. Such discharges add dye particles to these water bodies, bringing out, first, aesthetic deterioration due to the appearance of a visible color that covers the entire surrounding (Al-Tohamy et al., 2022; Castro et al., 2019). Secondly, and with more significant environmental repercussions, the presence of these pollutants diminishes underwater light transmission considerably, causing insufficient energy for the aquatic biota, which results in impaired photosynthesis. Besides, dyes are highly resistant to light, heat, and weather conditions given their aromatic structure, making dye-bearing water a great source of pollution, where concentrations as low as 1 ppm affect gas solubility, water transparency, and aesthetics of the environment (Li et al., 2025).

With an annual production exceeding 700,000 tons, synthetic dyes have become substances of massive use in several economic sectors. Particularly, Basic Red 46 (BR46), C.I.

110825, is a cationic dye with molecular formula $C_{18}H_{21}N_6$, a molecular weight of 401.3 g mol^{-1}. Because of its strong affinity for a wide range of fabrics, BR46 is commonly employed in the textile industry, and it is also utilized in the food and yeast trade. However, BR46 is classified as a highly toxic, mutagenic, and carcinogenic compound, immediate exposure may result in allergic reactions and skin irritation, indicating its potential risk to the human health (Castro et al., 2019; Pereira and Alves, 2012).

Currently, different physicochemical methodologies for dye-contaminated water treatment are available, such as filtration, a technique based especially on the use of polymeric membranes that allow the separation of pollutants through size exclusion processes (Robinson et al., 2001); ozonation, involves the application of ozone to break down organic compounds present in water, including dyes (Abrile et al., 2020); electrochemical methodologies that generate oxidizing species through the appliance of electric current, which degrades organic compounds due to electrochemical reactions (Aqeel et al., 2020); coagulation-flocculation is another alternative where coagulants are added to the contaminated water, which promotes the formation of flocs that trap dyes and other impurities, assisting their subsequent exclusion through sedimentation (Ihaddaden et al., 2022); and photocatalysis that is based on the activation of reactive oxygen species by ultraviolet radiation or visible light, which attack and degrade organic compounds (Saeed et al., 2022).

Despite its availability, most of these methodologies have drawbacks compared to adsorption. For instance, some of them require considerable investment in equipment and materials for their implementation on a larger scale, which may limit their applicability. In addition, several of these methods can generate by-products or secondary compounds that could be harmful to the environment (Shinde et al., 2024), underscoring the importance of considering the side effects of their application. Furthermore, some methods demand a lot of energy to operate (Aigbe et al., 2021), which could not only result in considerable financial costs but also raise concerns about long-term sustainability.

Adsorption is considered one of the most promising alternatives for dye-containing water treatment since it removes the pollutant without breaking down the molecule; it is efficient, fast and a cost-effective methodology (Pavithra et al., 2019). In this context, diverse agricultural byproducts have been explored as potential, eco-friendly, and non-conventional adsorbents. The use of such alternative materials has increased in recent years due to their wide availability, low cost and removal efficiencies greater than 90% (Crini, 2006; Echavarria-Alvarez et al., 2014; Gupta et al., 2009; Srinivasan et al., 2010).

Corn byproducts, such as cobs, leaves and husks, account for approximately 50% of the total mass of the plant. Hence, corn cobs (CC) are readily available as an agricultural byproduct. Particularly, in Colombia, geographical and wheather conditions have favored the corn production throughout the whole territory (Salgar, 2005). In this regard, the Ministry of Agriculture and Rural Development of Colombia, has reported approximately 1.38 million tons of corn produced in 2021 (Ministerio de Agricultura y Desarrollo Rural, 2021). Moreover, according to the United Nations Food and Agriculture Organization (FAO) (FAO, 2009), this product can be abundantly found in numerous countries, including the United States, Argentina, Brazil, and China, registering in 2020 a corn production that amounted 64.63% of the world production (Wang et al., 2021).

On the other hand, chemical oxygen demand (COD) is one of the parameters used to determine the degree of wastewater pollution. COD is the amount of oxygen needed to oxidize all oxidable compounds in the water through chemical means (Mañunga et al., 2010). In this work, the COD was quantified after the removal process to determine the extent to which this treatment improves the quality of dye-containing effluents. As expected, each country has regulations establishing the maximum COD values that effluents must meet before discharge. In the case of Colombia, the Ministry of Environment and Sustainable Development, through Resolution 631 of 2015, set the maximum allowable limits for liquid discharges to protect water resources and minimize environmental impacts caused by various industrial activities. For example, in the textile industry, discharges must have a COD of less than or equal to 400.00 mg O_2L^{-1}, total suspended solids (TSS) of up to 50.00 mg L^{-1}, and a biochemical oxygen demand (BOD) of 200.00 mg O_2L^{-1} (Ministerio de ambiente y desarrollo sostenible, 2015). According to the report by Área metropolitana Valle de Aburrá (2019), an evaluation conducted at strategic points along

the Medellín River revealed concerning levels in several water quality parameters. The maximum values recorded included a COD of 274.00 mg O_2L^{-1} , TSS of 298.00 mg L^{-1}, and a true color of 52.64 UPC. These findings reflect the combined impact of industrial, domestic, and agricultural discharges into the river. However, it is important to highlight that dye-bearing effluents, primarily from the textile industry, can significantly exacerbate these indicators if not properly treated, increasing the organic load, and affecting the appearance and quality of this vital water resource. In this context, the adsorption process emerges as one of the most effective and sustainable technologies for the removal of persistent pollutants, allowing a significant reduction in COD, TSS and dye-bearing contaminants.

The literature reports a substantial number of studies on the removal of BR46 dye using agricultural by-products. Most of these studies have successfully applied univariate approaches to evaluate the influence of individual operating parameters on adsorption performance. While this methodology has provided valuable insights into the adsorption behavior of BR46, it inherently focuses on one variable at a time, letting the remaining factors fixed. Consequently, potential interactions among operational parameters and their combined effect on process optimization have been less explored. A variety of agrowastes, such as coconut shells, sumac leaves, raw cactus fruit, pinecones, raw pomegranate, princess tree leaves, pine leaves, and olive pomace, have been reported for BR46 removal using univariate experimental designs (Akkari et al., 2023, 2024; Aldemir et al., 2023; Deniz et al., 2011; Graba et al., 2022; Jóźwiak et al., 2018; Kaouah et al., 2013). In addition, some studies have employed chemical or thermal modifications – commonly pyrolysis – to enhance adsorption capacity (Jabar et al., 2022; Kaouah et al., 2013), although these treatments may increase operational costs and processing complexity. Rice husk was also evaluated to remove BR46 using a statistical design, obtaining a removal of 95%, however, the study focused mainly on process optimization and did not include a comprehensive evaluation of adsorption kinetics, equilibrium, and thermodynamic behavior (Cueva-Orjuela et al., 2017).

Within this framework, this study focused on the removal of BR46 dye by implementing statistical tools for the first time to develop a more accurate, efficient, and reproducible adsorption model. Raw corn cob was selected as an alternative agricultural adsorbent, offering an environmentally sustainable process that promotes the use of waste materials without structural modification. Initially a 2^3 factorial design was conducted, followed by a narrowing design using the steepest ascent approach and, finally, an orthogonal central composite surface design was performed to determine the optimal conditions. In addition, kinetic, equilibrium, and thermodynamic studies were conducted to better understand the interaction between the adsorbent, CC, and the dye, BR46. These statistical tools provided valuable insights for the future scale-up of the process. Finally, water quality after the removal process was also assessed by measuring the COD.

MATERIALS AND METHODS

Preparation of BR46 solution

BR46, with a purity greater than 99%, was obtained from Colorquímica S.A, a local dye company in Medellín, Colombia. A standard BR46 solution with concentration 100 mg L^{-1} in distilled water was prepared, which was used to perform a calibration curve on a Perkin-Elmer Lambda 35 UV-Vis spectrophotometer under the dye's maximum absorbance wavelength, namely λ_{max} = 531.9 nm. The structure of this azo dye is shown in Figure 1.

Agricultural by-product pretreatment

Corn cobs (CC) were obtained from a local market in Medellín, Colombia, and underwent a milling and sieving process to achieve a particle size in the range 300 to 500 μm. This particle size was selected since it was found to be the most suitable according to previous studies (Zuluaga Díaz et al., 2014) and related works (Trivizadakis et al., 2006). Furthermore, the specific surface area of the CC was determined to be 79.16 $m^2\ g^{-1}$, as reported in previous research (Velandia-Ciendua et al., 2019). Subsequently, the material underwent five consecutive washes with distilled water until the wash water was clear. The washed material was then dried in a forced convection oven at 70 °C for 48 hours and stored in airtight containers for subsequent experimental use.

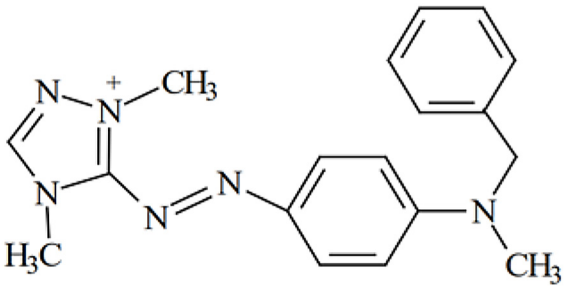

Figure 1. Chemical structure of BR46 dye

Characterization of raw CC

Determination of point of zero charge

The point of zero charge (PZC) corresponds to the pH value at which the surface net charge of an adsorbent is electrically neutral. The PZC for CC was determined by mass titration, using distilled water solutions adjusted to three initial pH levels (3.0, 7.0, and 11.0) by the addition of HCl and NaOH. For each pH condition, the change in pH was measured after 24 hours of contact with continuous stirring at 130 rpm, using six different CC dosages ranging from 10 to 120 g·L^{-1}. All experiments were carried out in triplicate at room temperature using a Unimax 1010 shaker. pH measurements were taken with a Schott pH meter. The PZC corresponds to the pH value approached by the system as the adsorbent dosage increases.

FTIR spectral analysis

To identify the functional groups of greater participation in the adsorption process, spectra of the CC samples were taken before and after the removal of BR46 in the range of 4000–500 cm^{-1} with a resolution of 2 cm^{-1}. This analysis was carried out in a Perkin Elmer spectrometer with attenuated total reflectance Fourier-transform infrared (ATR FT-IR) spectroscopy, Spectrum Two.

Study of BR46 adsorption through factorial and response surface designs

The adsorption process was conducted under a discontinuous system, using 50 mL Erlenmeyer flasks with the respective dosage of CC and 50 mL of BR46 solution with the corresponding concentration for each experimental test. The Erlenmeyer flasks were stirred in a Unimax 2010 Shaker at 180 rpm. Once the contact time was over, the dye-impregnated material was separated from the residual solution by filtration. To calculate the removal capacity, the absorbances of the starting and remaining solutions were measured with a Perkin Elmer UV-Vis Lambda 35 spectrophotometer at 531.9 nm. The response variable was removal, calculated as stated in Equation 1, where C_0 and C_f correspond to initial and final solution concentrations, respectively.

$$\%Rem = \frac{C_0 - C_f}{C_0} \times 100\ \% \qquad (1)$$

Full factorial and narrowing design

A 2^3 factorial design with a central point was conducted to evaluate the factors dosage (D), contact time (T), and initial dye concentration (C_0), at the levels indicated in Table 1, using a fixed solution volume of 50 mL. Based on prior analyses, the following variables were kept constant because of their minimal influence on the adsorption process: pH of 7.0, particle size of 300–500 µm, temperature of 25 °C, and stirring speed of 180 rpm. A 100 mg L^{-1} BR46 dye solution was prepared, and dilutions were made to get concentrations of 10, 25, and 40 mg L^{-1}.

The narrowing design uses the steepest ascent path to evaluate the response variable in the gradient's direction to have a closer estimation of the optimum conditions (Kowalski et al., 2005). In this case, dosage steps of 0.5 g L^{-1} were taken since this factor was the most significant in the factorial design. Steps in the other factors were determined according to their effect using Statgraphics 19 software. The conditions of each experiment are listed in Table 3. A negative control was performed for each experimental test with the corresponding dosage of CC and 50 mL of distilled water. All experiments were carried out at pH 7.0, with a stirring speed of 180 rpm, and in triplicate.

Central composite response surface design

A central composite response surface design was carried out with conditions close to the maximum removal found in the narrowing design. The levels and the corresponding values for each factor are shown in Table 1. A negative control was performed for each dosage value. The maximum removal conditions were established using Statgraphics 19. Finally, the optimal removal, determined by the previous surface design, was evaluated in quintuplicate and compared to the removal predicted by the model.

Table 1. Factors and levels for the 2^3 factorial design and the central composite surface design on the removal of BR46-CC system

Factor	2^3 factorial design			Central composite surface design				
	Level			Level				
	Low	Medium	High	-1.68179	-1	0	1	1.68179
T (min)	60	150	240	191.1	195.2	201.3	207.5	211.5
C_0 (mg L^{-1})	10	25	40	13.3	14.1	15.2	16.4	17.2
D (g L^{-1})	1.0	2.5	4.0	4.5	4.7	5	5.3	5.5

Chemical oxygen demand (COD) determination

The COD of the aqueous solution was determined before and after BR46 removal, under the optimal conditions found in the response surface design. A negative control experiment using distilled water and CC was also evaluated. A standard solution of potassium hydrogen phthalate with a COD of 500 mg O_2L^{-1} was used to perform a calibration curve. The methodology for this assessment corresponds to that described by Supelco (2020). The measurements were performed by adding 0.30 mL of Perkin-Elmer Spectroquant solution A, 2.30 mL of Perkin-Elmer Spectroquant solution B, and 3.0 mL of the sample in a 16 mm corrosion and temperature resistant screw lid cuvette. The samples were heated to 148 °C for 120 minutes in a Perkin-Elmer Spectroquant TR-420 thermoreactor. After this time, the samples were allowed to cool down, then they were manually shaken, and the COD was measured in a Perkin-Elmer UV-Vis Lambda 35 spectrophotometer at 605 nm and 585 nm. For this method, a limit of detection (LOD) of 6 mg O_2L^{-1} has been indicated (ISO, 2002).

Kinetics of BR46 adsorption

The adsorption kinetics were evaluated using 50 mL Erlenmeyer flasks under the optimal adsorption conditions, previously found in the central composite response surface design. These Erlenmeyer were sealed and placed in a Unimax 2010 shaker with an incubator to keep the temperature constant throughout the process at a stirring speed of 180 rpm. These solutions were monitored for 240 min with contact times ranging from 0 to 240 min at 298 K. These samples were measured at the maximum absorption wavelength and in triplicate to establish the residual dye concentration.

Three nonlinear models were used to fit the data from the kinetics experiment, namely, pseudo-first order, pseudo-second order, and Elovich model.

Pseudo-first order kinetics

This model proposed by Lagergren in 1898 is one of the most widely used and is defined by Equation 2.

$$\frac{dq}{dt} = k_1(q_{eq} - q) \tag{2}$$

where: q_{eq} represents the amount of adsorbate transferred to the adsorbent surface at equilibrium (mg g^{-1}), while q represents the amount transferred (mg g^{-1}) at time t, k_1 denotes the rate constant expressed in min^{-1}.

By integrating Eq. (2), a closed form is obtained as shown in Equation 3.

$$q = q_{eq}(1 - e^{-k_1 t}) \tag{3}$$

Pseudo-second order kinetics

Pseudo-second order kinetics is another frequently used model and has been extensively reported in adsorption-related experiments (Wang and Guo, 2020a). This model is defined by Equation 4.

$$\frac{dq}{dt} = k_2(q_{eq} - q)^2 \tag{4}$$

An integration of Equation 4 yields Equation 5.

$$q = q_{eq}\left(1 - \frac{1}{k_2 q_{eq} t + 1}\right) \tag{5}$$

where: k_2 denotes the rate constant in g mg^{-1}.

Elovich kinetics

The Elovich kinetic model is an empirical model that states that activation energy increases

as the adsorption process is conducted and that the adsorbent surface is heterogeneous (Wang and Guo, 2020a). The mathematical expression that describes this model is presented in Equation 6.

$$\frac{dq}{dt} = ae^{-bq} \tag{6}$$

The integrated form of Equation 6 is Equation 7.

$$q = \frac{\ln(abt + 1)}{b} \tag{7}$$

where: a represents the initial adsorption rate in milligrams per gram per minute mg g^{-1} min^{-1} and b has units grams per milligram g mg^{-1}.

Adsorption isotherms for the BR46-CC system

The isotherm experiments were performed using 50 mL Erlenmeyer flasks, CC dosage was kept constant at 5.0 g L^{-1}, initial dye concentration was 10, 20, 40, 60, 80, 100, 120 and 150 mg L^{-1} and the contact time was set at 24 h. The experiments were performed in triplicate at temperatures 298, 318, and 328 K. Particularly, Langmuir, Freundlich, Redlich-Peterson, Langmuir-Freundlich, and Temkin models were evaluated in this work.

Langmuir model

In the Langmuir model, the surface is assumed to be homogeneous, and the adsorbed molecules are retained in a monolayer on the surface. The surface has a finite number of identical adsorption sites so that one molecule is retained in each of the sites. Also, this model neglects molecule interaction and is denoted as follows (Langmuir, 1916).

$$q_e = Q_{max}\frac{K_L C_e}{1 + K_L C_e} \tag{8}$$

where: Q_{max} is the maximum capacity of adsorption for the system under the experimental conditions (mg g^{-1}), K_L is a parameter indicating the affinity of the adsorbate for the adsorbent (L mg^{-1}), q_e is the amount of dye adsorbed at equilibrium per unit mass of adsorbent (mg g^{-1}), and C_e is the concentration of the adsorbate in equilibrium (mg L^{-1}).

Freundlich model

Freundlich adsorption isotherm model characterizes the process as reversible and non-ideal. Freundlich model is not restricted to monolayer formation, thus it's also applicable to multilayer adsorption. This model also works when adsorption heat and affinities are not uniformly distributed in a heterogeneous surface (Al-Ghouti et al., 2020). Freundlich model is given by Equation 9.

$$q_e = K_F(C_e)^{\frac{1}{n_F}} \tag{9}$$

where: K_F is a parameter related to the affinity of the system ($mg^{1-1/nF}g^{-1}\,L^{1/nF}$), while n_F is the Freundlich constant that indicates the adsorption intensity (non-dimensional).

Redlich-Peterson model

Redlich-Peterson is a model describing adsorption in a real system, considering multilayer formation and interaction among adsorbed particles. It is a combination of Freundlich and Langmuir models incorporating 3 parameters (Al-Ghouti et al., 2020). This model is presented in Equation 10.

$$q_e = \frac{\alpha C_e}{1 + \beta C_e^{\gamma}} \tag{10}$$

The equation comprises three empirical coefficients denoted as α, β, and γ. The exponent γ within the equation typically falls within the range of 0 to 1.

Langmuir-Freundlich model

The Langmuir-Freundlich isotherm, also known as the Sips model, constitutes a fundamental tool in the analysis of the homogeneity or heterogeneity of adsorption systems (Wang and Guo, 2020b). However, it has a limitation associated with non-adherence to Henry's law when the adsorbate concentration is extremely low or under low pressure conditions (Al-Ghouti et al., 2020). The Sips isotherm is defined by Equation 11 (Wang and Guo, 2020b).

$$q_e = \frac{A_s C_e^{n_s}}{1 + K_s C_e^{n_s}} \tag{11}$$

where: A_s ($mg^{1-n_s}g^{-1}L^{n_s}$), K_s ($L^{n_s}\,mg^{-n_s}$) and n_s are the parameters of the Langmuir-Freundlich isotherm.

Temkin model

The Temkin isotherm describes a multilayer adsorption process (Pérez-Marín et al., 2007). This approach considers the interaction between the adsorbent and the adsorbate, disregarding the dependence on concentration values (Dada et al., 2012; Hameed et al., 2008; Wang and Guo, 2020b). The Temkin model is presented by Equation 12.

$$q_e = \frac{RT}{b_t}\ln(K_t) + \frac{RT}{b_t}\ln(C_e) \qquad (12)$$

The constants K_t and b_t represent the Temkin constants.

Thermodynamic parameters

Thermodynamic properties play a fundamental role in an adsorption process given that they determine its spontaneity. Both entropy (ΔS°) and enthalpy (ΔH°) are necessary considerations in calculating the Gibbs free energy ΔG°. If ΔG° is negative at a given temperature, the reaction occurs spontaneously. Adsorption is classified as exothermic if ΔH° is negative, and as endothermic, if ΔH° is positive. The magnitude of the ΔH° also indicates whether the process is physisorption or chemisorption (Tran et al., 2021). The affinity of the adsorbent towards the adsorbate is quantified by an increase in the value of $\Delta S°$ (Al-Ghouti et al., 2020).

The estimation of thermodynamic parameters was carried out according to the methodology described by Chen et al. (2021). Thus, the reaction mechanism considered depends on the selected isotherm. The general reaction mechanism is given by Equation 13.

$$mS + nA \leftrightarrow pS - A \qquad (13)$$

where: S is the surface, A is the adsorbate, and $S - A$ is the adsorption complex. m, n, and p are stochiometric coefficients.

The experimental equilibrium constant related to this general mechanism is presented in Equation 14.

$$K_{exp} = \frac{{q_{eq}}^{p}}{\left(q_{max} - q_{eq}\right)^{m}\left(C_{eq}\right)^{n}} \qquad (14)$$

However, the equilibrium constant must be dimensionless to be used in the calculation of thermodynamic properties. To achieve this, the standard state is implemented. Thus, the dimensionless equilibrium constant is given by the Equation 15.

$$K_{eq} = K_{exp}\,(q^0)^{m-p}(C^0)^n \qquad (15)$$

where: q^0 and C^0 represent the charge and concentration at standard conditions respectively.

The relationship between the equilibrium constant and the Gibbs free energy is given by Equation 16.

$$\Delta G^0 = -RT\ln K_{eq} \qquad (16)$$

where: ΔG^0 is the Gibbs free energy at standard conditions (J mol^{-1}), R is the universal constant of gases (8.314 J mol^{-1} K^{-1}), T is the absolute temperature (K) and K_{eq} is the equilibrium constant of the system.

According to the Van't Hoff equation, the relationship between the equilibrium constant and the temperature, assuming low variations of ΔH^0 and ΔS^0 with temperature is given by Equation 24 (Atkins, 2022).

$$\ln K_{eq} = -\frac{\Delta H^0}{RT} + \frac{\Delta S^0}{R} \qquad (17)$$

The Gibbs free energy is also given by Equation 18.

$$\Delta G° = \Delta H° - T\Delta S \qquad (18)$$

RESULTS AND DISCUSSION

Characterization of raw CC

Determination of PZC

The results obtained by mass titration are shown in Figure 2a. As depicted, the final pH values approach 5.5 as the dosage increases. It is worth noting that this value is not affected by the initial pH used in the experiment, indicating that the PZC is an intrinsic property of the adsorbent material.

FTIR spectral analysis

ATR FTIR spectroscopy analysis was performed to identify the functional groups present in CC, as well as to observe possible changes in its structure after BR46 dye removal, shown in Figure 2b.

A strong band is observed at 3338 cm^{-1} in CC corresponding to the stretching of the OH bond associated with hydroxyl functional groups

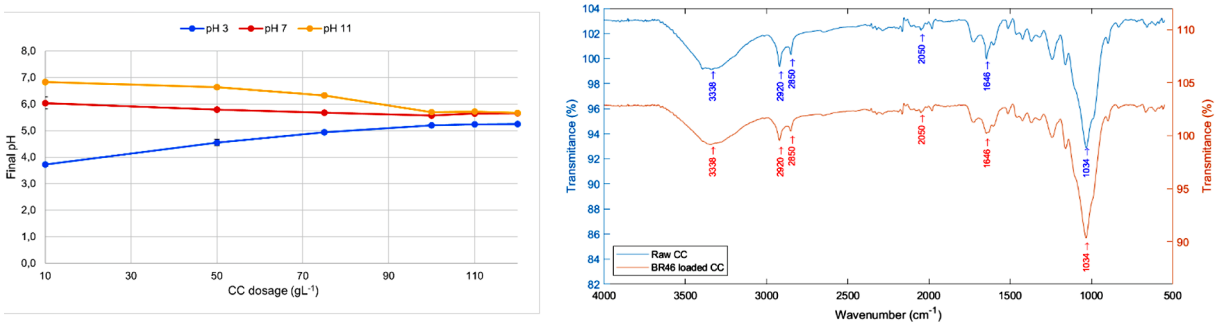

(a) **(b)**

Figure 2. (a) PZC by mass titration. (b) FTIR spectra before and after adsorption

(Smith, 2018). Bands at 2920 and 2850 cm^{-1} are attributed to the vibrations of the CH bond. Then, small bands appear between 1910 and 2050 cm^{-1} for the aromatic fingerprints. Medium intensity bands, between 1500 and 1680 cm^{-1}, are associated with the C-C double bonds and the CO bond, which are present as carboxyl groups in the glucuronic acid of hemicellulose and the C=O stretching in conjugated carbonyl groups of lignin (Fan et al., 2012). Finally, an intense band is registered at 1034 cm^{-1} which correlates with the vibration of the C-O-C bond in ethers (Smith, 2018). Figure 2b corresponds to the CC-BR46 system, changes in the adsorption bands with a more rounded shape for the OH bond vibration at 3338 cm^{-1} and a higher intensity of the remaining bands are observed, indicating the interaction between CC and BR46.

Statistical design of experiments

Factorial design and narrowing design

The analysis of variance (ANOVA) for the 2^3 full factorial design of BR46 adsorption onto CC is represented by the Pareto chart in Figure 3a, in which the factors are arranged in order of their statistical significance. It was found that the most significant factor is the adsorbent dosage, with a positive effect on the removal percentage, followed by the initial dye concentration with a negative effect and in the third place, the contact time with a positive effect. Furthermore, the interaction *DC* also had a significant positive effect, while the interaction *TD* had a significant negative effect. The remaining interaction *TC* did not have a statistically significant effect on the BR46 dye removal percentage. The presence of significant interactions shows that this system's behavior is non-linear and as such, univariate approaches are not ideal. Besides, the non-linearity suggests there might be optimal operating conditions for the system. The interaction plot presented in Figure 3b confirms the assertions obtained from the pareto chart in Figure 3a.

According to the Tukey's multiple range test, which are denoted with a lower-case superscript letter, the pairs of treatments (4,5), (2,7), and (3,8) belong to the same homogeneous groups, so there is not any statistical difference among these pairs of experiments. The conditions for each treatment and their corresponding final removal percentages are displayed in Table 2.

The highest removal percentage of 92.70% was obtained in treatment 5 under the following conditions, 240 min of contact time, 10 mg L^{-1} of initial dye concentration, and 4.0 g L^{-1} of CC dosage. However, this treatment has no statistical difference with treatment 4, which achieved a similar removal percentage and shared the same values in dosage and contact time but with a higher initial concentration of BR46. This shows that under the specified values of time and dosage, the performance is similar when changing the initial dye concentration, and since one of the objectives of this research is to retain the highest feasible dye load, the possibility of optimization is opened.

The following mathematical model fit the data in Table 2 with $R^2 = 0.9457$

$$\%\ \text{Rem} = 64.057 + 5.3082T + 6.5313D - \\ - 0.7360C - 1.0043TD + 0.1663DC$$

where: T is the contact time in min, D is the adsorbent dosage in g L^{-1}, and C is the initial dye concentration in mg L^{-1}.

This high R^2 value shows that it's suitable for approximating the expected removal within the evaluated interval $60 \leq T \leq 240{,}1 \leq D \leq 4{,}10 \leq$

$C \leq 40$). Besides, the presence of nonlinear terms indicates that interactions are relevant.

Afterwards, a narrowing design was implemented to obtain better conditions for the process. In this design, we started from the center of the region assessed in the previous factorial design and evaluated it in a path following the gradient (Kowalski et al., 2005). Subsequently, an orthogonal central composite surface design was performed, which consisted of focusing on this narrower region to develop its mathematical model and determine the optimal point. In Figure 4, a diagram of the evaluated areas is shown, whose methodology is based upon line-search methods of optimization.

Table 3 shows the average removal percentages obtained for each one of the 11 experiments of the narrowing design. It is observed that the highest removal percentage of BR46 was in the order of 97.3 ± 0.2% and corresponds to treatment 6, under a dosage of 5.0 g L^{-1}, a contact time of 201.3 min, and an initial BR46 concentration of 15.2 mg L^{-1}. This value is quite satisfactory; it represents an increase of approximately 5% compared to the adsorption efficiency obtained in the factorial design but achieved in this case in a shorter time and with a higher load of RB46. However, in search of greater optimization it was decided to carry out the central composite surface design with level 0 of all the factors under these conditions and with values for the α and -α levels corresponding to the adjacent experiments to this maximum (Table 1).

The standard deviation presented in Table 3 validates the consistency and precision of the obtained results. The maximum observed value was 1.67%, indicating that the data is reliable and adequately represents the BR46-CC system. In particular, the standard deviation for the highest removal percentage was 0.16%, calculated from all replicates of experiment number 6. This finding points out that the result, with an average value of 97.3% removal, is highly precise and reliable.

Central composite response surface design

Adsorption experiments were conducted as specified in Table 1. In agreement to the analysis performed in Statgrafics 19, a local maximum was found within the evaluated range and, according to the model structure, it's also a global

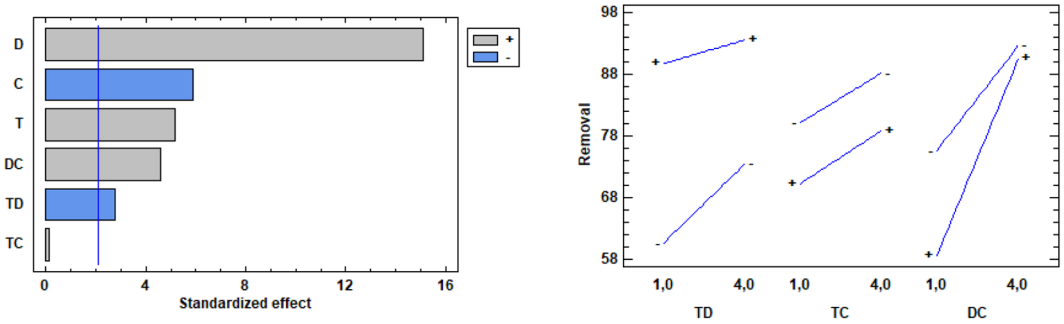

Figure 3. (a) Pareto chart for 2^3 full factorial design, (b) interaction plots

Table 2. Experimental removal percentages for the 2^3 full factorial design for the BR46-CC system

Exp	T (min)	C (mg L^{-1})	D (g L^{-1})	Removal (%)
1	60	40	1.0	51.63 ^{f}
2	150	25	2.5	88.09 ^{c}
3	240	40	1.0	63.32 ^{e}
4	240	40	4.0	92.28 ^{a}
5	240	10	4.0	92.70 ^{a}
6	60	10	4.0	90.53 ^{b}
7	60	40	4.0	86.71 ^{c}
8	60	10	1.0	67.50 ^{e}
9	240	10	1.0	81.63 ^{d}

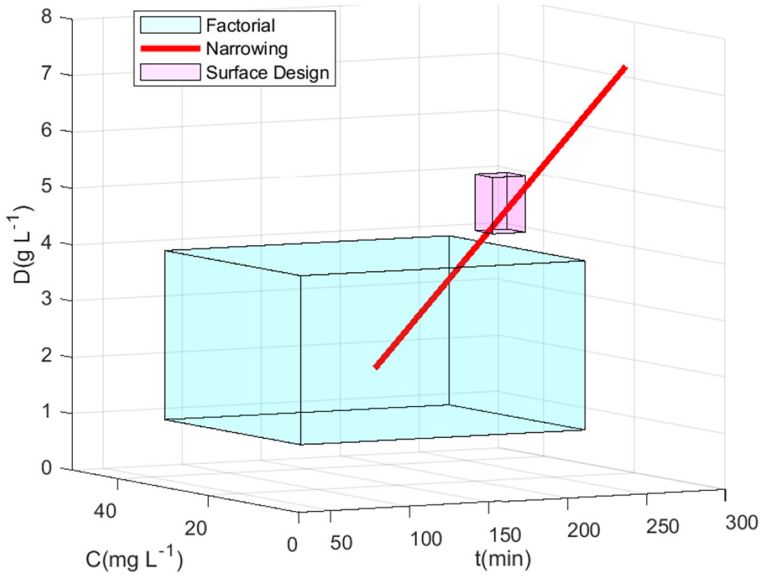

Figure 4. Scheme of evaluated zones with experimental designs

Table 3. Conditions for narrowing design on the removal of the BR46-CC system

Exp	T (min)	C (mg L^{-1})	D (g L^{-1})	Removal (%)	Std dev. (%)
1	150.0	25.0	2.5	87.14	0.33
2	160.3	23.0	3.0	90.06	0.28
3	170.5	21.1	3.5	91.23	0.82
4	180.8	19.1	4.0	93.42	0.04
5	191.1	17.2	4.5	94.36	0.59
6	**201.3**	**15.2**	**5.0**	**97.25**	**0.16**
7	211.6	13.3	5.5	94.69	1.67
8	221.9	11.3	6.0	94.98	1.05
9	232.1	9.4	6.5	95.89	0.62
10	242.4	7.4	7.0	95.76	0.59
11	252.6	5.4	7.5	96.39	0.89

maximum. The optimal operating conditions correspond to *D* at level 1.68178 (nominal value = 5.5 g L^{-1}), *C* at level 1.18366 (nominal value = 16.60 mg L^{-1}) and *T* level 0.1034576 (nominal value = 201.93 min) with a predicted removal of 94.86%. These operating conditions were experimentally evaluated in quintuplicate way, achieving removals of 97.6%, 95.7%, 99.1%, 99.3% and 98.9%. The average removal level was 98 ± 1%, which is higher than predicted and surpasses the results obtained in any other previous work. Thus, these conditions were taken as optimal and will be used for subsequent experiments in this study.

Although the contact time under optimized conditions is 201.93 min, this value is comparable to those reported for other lignocellulosic biosorbents employed for dye removal from aqueous solutions (Yadav et.al., 2024). From an industrial perspective, adsorption processes are frequently operated in batch or continuous systems, where process feasibility is mainly governed by adsorption capacity, removal efficiency, and operational cost rather than equilibrium time alone. In this context, the use of raw corn cob as an untreated, low-cost, and abundantly available agricultural residue represents a significant advantage, supporting the potential applicability of the proposed process for wastewater treatment.

Additionally, if contact time represents a limiting factor in industrial application, a removal of 90.53% was achieved in 60 min under the conditions of experiment 6 (Table 2). Adsorbent regeneration and reuse were not evaluated in the present study and therefore constitute a limitation of

the proposed process. Nevertheless, given the lignocellulosic nature of raw corn cob and previous reports on the reusability of similar agricultural residues, regeneration and multi-cycle adsorption performance are considered feasible and should be addressed in future studies to further assess the long-term applicability of the system.

Figure 5 shows the response surface of the obtained model for this system. As it comprises 3 factors and a response variable, one of those factors must be fixed for it to be graphically shown. *D*, *C*, and *T* are fixed at their optimum values in Figures 5a, 5b and 5c respectively. In all cases, negative curvature is observed, proving the fact that the system yields optimal results at this operation point.

These results showed a 1% increase compared to the data previously obtained using the narrowing design, pointing out that the narrowing design really accelerates and facilitates the identification of the most efficient improvement path. Furthermore, it is worth highlighting that the application of the central composite response surface design allowed the mathematical validation of the optimal point for experimental design.

Evaluation of chemical oxygen demand (COD)

The result obtained for COD was highly satisfactory as an effective parameter to determine an improvement in water quality after the removal process. Thus, from an initial COD of 127.80 mg O_2 L^{-1}, a final COD of 90.80 mg O_2 L^{-1} was registered, achieving a decrease in organic load of 37 units, that is a 29% reduction in the COD level, which is quite significant, pointing out that the treatment of colored effluents through removal with non-conventional adsorbents, represents an efficient, economical, sustainable, and environmentally friendly option that truly helps to improve water quality. This reduction in COD after BR46 adsorption indicates an improvement in water quality associated with the removal of organic dye molecules. However, it is not intended to imply compliance with discharge regulations, as COD limit values vary among countries and depend on local environmental legislation as discussed in the Introduction. Adsorption using raw corn cob should therefore be considered as a complementary or preliminary treatment step rather than a standalone solution. Nevertheless,

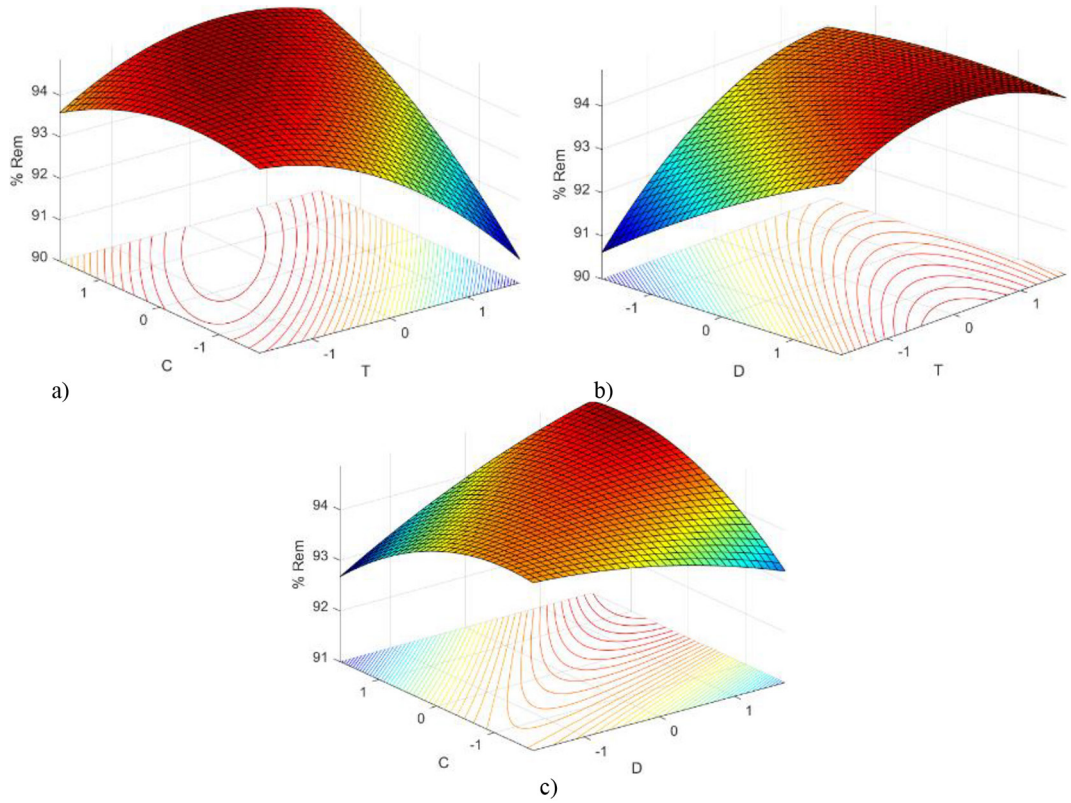

Figure 5. Central composite response surface with dosage fixed at optimal condition for the BR46-CC system: a) surface response with *D* fixed at optimum, b) surface response with *C* fixed at optimum, c) surface response with *T* fixed at optimum

the obtained COD decrease confirms the contribution of the adsorption process to reducing the organic load of dye-contaminated wastewater.

It should be mentioned that this is one of the few works where, after optimizing the adsorptive process, the improvement in water quality is demonstrated by measuring COD. On the other hand, the ease and speed of this test would allow companies that generate dye-bearing effluents to have an accurate criterion for discharging their industrial effluents in accordance with established legislation. As far as we know, Kaouah et al. (2013) report the measurement of COD but under another methodology, using an automated COD analyzer. In that work, the COD of a real effluent containing three dyes was measured, which didn't include BR46. Therefore, there are no reports to compare with our findings.

Adsorption kinetics of BR46-CC

Table 4 presents the experimental data of the adsorption kinetics for the BR46-CC system at 298 K under the best conditions of the process: a dosage of 5.5 g L^{-1}, an initial concentration of 16.6 mg L^{-1}, and a contact time of 201.93 min. The selection of the most appropriate model was based on the criteria of best correlation fit (R^2) and the lowest sum of the squared errors (SSE).

As can be seen in Table 4, the experimental data show a better fit with the pseudo-second-order model, with a correlation coefficient $R^2 = 0.94$ and an SSE of 0.03. This R^2 value indicates that the system corresponds to a chemisorption process (Zheng et al., 2010). For its part, the Elovich model displays a R^2 with a value 8.7 % lower than the best fit value, while the Pseudo-first order kinetic model had a poor adjustment with an R^2 value of 0.59.

It is worth mentioning that research related to the BR46 removal reports similar results in terms of the best fit with the pseudo-second-order kinetic model, which is consistent with the findings of the present work. For instance, Akter et al. (2021) reported a correlation coefficient of $R^2 = 0.99$ using banana peel as an adsorbent. Similarly, Akkari et al. (2023) obtained a correlation of $R^2 = 0.99$ when employing raw pomegranate peel as an adsorbent. Other studies using adsorbents such as princess tree leaf (Deniz et al., 2011), olive pomace (Graba et al., 2022), and pinecone (Aldemir et al., 2023) have also documented high correlations with this kinetic model. It is important to highlight that the pseudo-second-order kinetic model is predominant in the adsorption processes of different dyes on low-cost agricultural waste (Bushra et al., 2021). The plot of the three kinetic models used to evaluate the BR46-CC system is shown in Figure 6.

In the adsorption kinetics, it is observed that during the initial 20 minutes, the value of q_t increases rapidly. Subsequently, the rate of increase in q_t slows considerably until approximately minute 100. From this point onward, the value of q_t finds stability, indicating that the system has reached adsorption equilibrium.

Adsorption isotherms of BR46-CC

The results obtained from adjustment of the five equilibrium models with their respective parameters at the three temperatures for the adsorption of BR46 onto CC are summarized in Table 5. In general, a good adjustment is seen with all the evaluated models. Figure 7 shows the experimental data and the model fitting for temperatures at 298, 308, and 318 K, respectively.

In particular, the best fit was found with Redlich-Peterson model (R-P), with a correlation coefficient $R^2 = 0.999$ at 298 K, $R^2 = 0.995$ at 318 K, and $R^2 = 0.999$ at 328 K, which explains that the system follows a combined mechanism and not ideally a monolayer adsorption and the existence of interactions between the adsorbed particles (Tran et al., 2021). The second-best fit is observed with the Langmuir-Freundlich model (L-F), with correlation coefficients R^2 of 0.998; 0.994 and 0.998 at 298 K,

Table 4. Kinetics results for the CC-BR46 system

Model	K_1 (min^{-1})	q_e (mg g^{-1})	SSE	R^2
Pseudo-first order	1.55	2.82	0.19	0.59
Pseudo-second order	K_1 (min^{-1})	q_e (mg g^{-1})	SSE	R^2
	1.29	2.86	0.03	0.94
Elovich	a (mg g^{-1} min^{-1}	b (g mg^{-1})	SSE	R^2
	8.65×10^{11}	12.02	0.07	0.84

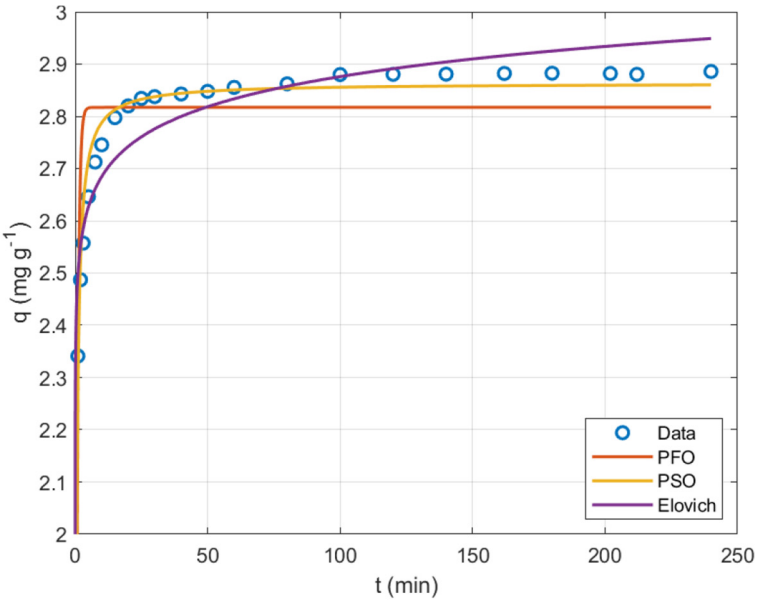

Figure 6. Kinetic models used to evaluate the BR46-CC system: PFO – pseudo-first order, PSO – pseudo-second order

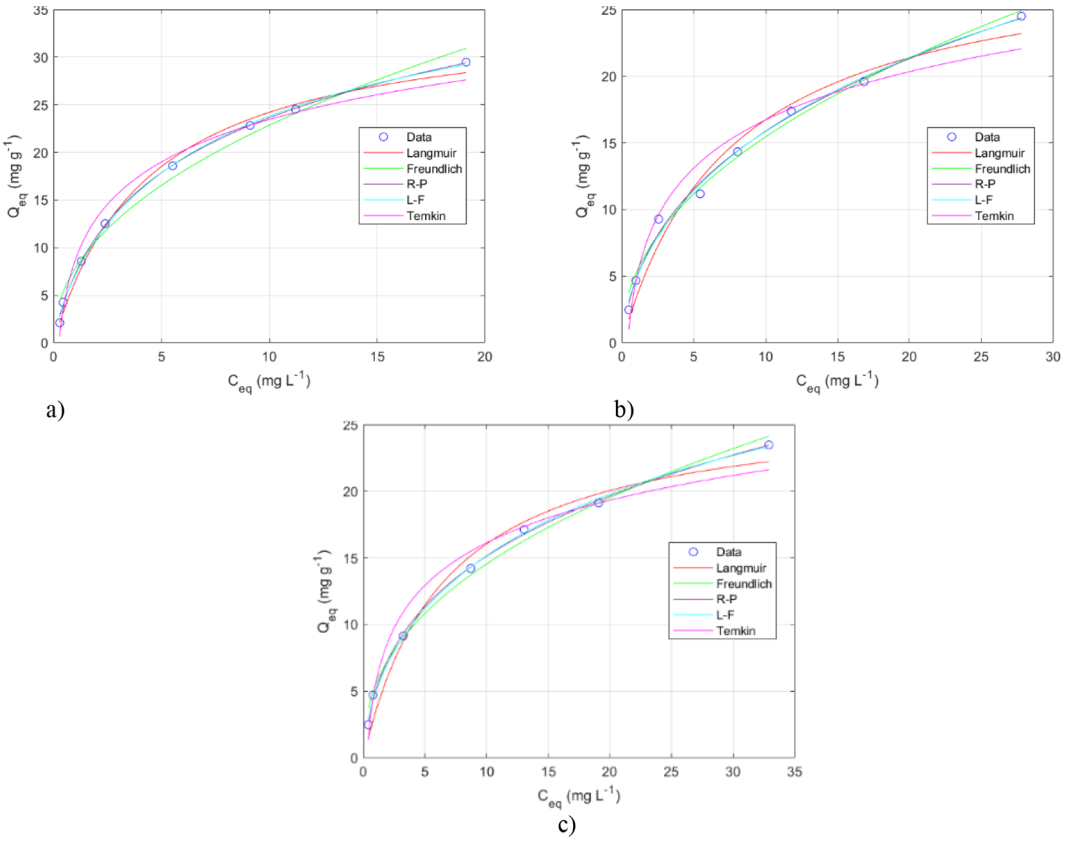

Figure 7. Isotherms at different temperatures: a) isotherm comparison at 298 K, b) isotherm comparison at 318 K, c) isotherm comparison at 328 K

318 K, and 328 K, respectively, pointing out the heterogeneity of the system, according to a more real process. This good adjustment of the different isotherms is also mentioned when BR46 was removed onto activated carbon from wild olive cores (Kaouah et al., 2013).

Moreover, the Freundlich isotherm also showed an excellent correlation for all evaluated

temperatures, with R^2 greater than or equal to 0.988, placing itself in the third-best fit. Notably, as the temperature increased, the model fitting improved, suggesting that this model adequately describes the process, especially at elevated temperatures.

On the other hand, the Langmuir isotherm ranked fourth with $R^2 = 0.987$, indicating that the system has a behavior similar to monolayer adsorption, which is also supported by the Freundlich isotherm fit with a value of $n_F > 1$. It is also observed that the good correlation for the Langmuir isotherm at 298 K ($R^2 = 0.995$) decreases as the temperature increases ($R^2 = 0.983$ at 313 K). This behavior can be explained by the fact that q_m decreases as the temperature increases, obtaining greater surface coverage that allows some molecules to be fixed by physisorption as they approach the total coverage of the monolayer. This hypothesis is reinforced by the increase in the fitness of the Freundlich isotherm at high temperatures since this model can fit combined mechanisms better than Langmuir.

Additionally, even with a good fit, the Temkin model earns fifth place with an average $R^2 = 0.971$ for the three evaluated temperatures. This isotherm model considers chemisorption in which the adsorption enthalpy of the molecules decreases linearly with the surface's coverage. This isotherm had a slightly lower fit than the Langmuir model, indicating that the adsorption enthalpy is constant or decreases very little.

Finally, the Redlich-Peterson and Langmuir-Freundlich isotherms are designed to take characteristics of the Langmuir and Freundlich isotherms, interpolating between them. These models had a marginally better fit than the Langmuir isotherm. It is important to mention that in the Redlich-Peterson isotherm the value of γ is 0.79, indicating that this model is closer to the Langmuir isotherm, which corresponds to a value of $\gamma = 1$.

The results of this study are consistent with previous research. For example, (Jóźwiak et al., 2018, 2021) reported good adequacy of the Langmuir isotherm using coconut shells and hen feathers. Kiani et al. (2021) found that the Langmuir isotherm adequately describes the adsorption equilibrium of BR46 on activated carbon from palm, while the studies using olive pomace (Graba et al., 2022), and raw cactus fruit peels (Akkari et al., 2024), have highlighted the ability of the Freundlich model to fit the system, better reflecting the combined adsorption mechanisms on heterogeneous surfaces.

Thermodynamic parameters of BR46-CC adsorption

The estimation of the thermodynamic properties was performed following the procedure referred to in section: Adsorption isotherms for the BR46-CC system. The Redlich-Peterson and Langmuir-Freundlich isotherms were the ones that presented the best fit at all temperatures. However, these models are empirical interpolations between the Langmuir and Freundlich models and, therefore, have no associated mechanism, preventing them from being used for the calculation of thermodynamic properties. Among the remaining models, Freundlich's is the one that best adjusts to more temperatures. For this reason, it was decided to use it for the calculation of thermodynamic properties. The specific Freundlich mechanism corresponds to Equation 14 with values $m = 0$, $n = 1$ and $p = n_F$. The values of the thermodynamic parameters and the equilibrium constant are shown in Table 6.

Table 5. Parameters of adsorption isotherms for the CC-BR46 system

Model	Temperature: 298 K					Temperature: 318 K					Temperature: 328 K				
Langmuir	Q_{max}	K_L	-	SSE	R^2	Q_{max}	K_L	-	SSE	R^2	Q_{max}	K_L	-	SSE	R^2
	34.9519	0.2252	-	4.3495	0.9957	29.6279	0.1297	-	10.2675	0.9837	26.7028	0.1508	-	10.2675	0.9837
Freundlich	K_F	n_F	-	SSE	R^2	K_F	n_F	-	SSE	R^2	K_F	n_F	-	SSE	R^2
	7.7965	2.1416	-	11.6995	0.9881	5.2574	2.1361	-	4.2019	0.9925	5.4742	2.3553	-	2.9412	0.9945
Langmuir-Freundlich	A_s	K_s	n_s	SSE	R^2	A_s	K_s	n_s	SSE	R^2	A_s	K_s	n_s	SSE	R^2
	8.4270	0.1905	0.7867	1.1497	0.9988	5.1962	0.0840	0.6144	2.7539	0.9949	5.5073	0.1157	0.6065	0.5972	0.9988
Redlich-Peterson	α	β	γ	SSE	R^2	α	β	γ	SSE	R^2	α	β	γ	SSE	R^2
	11.8570	0.6479	0.7924	0.5707	0.9994	11.4240	1.3938	0.6482	2.2973	0.9958	12.2279	1.4379	0.6923	0.4523	0.9991
Temkin	K_t	b_t	-	SSE	R^2	K_t	b_t	-	SSE	R^2	K_t	b_t	-	SSE	R^2
	3.8465	385.67	-	13.4643	0.9809	2.4732	507.18	-	15.6586	0.9602	3.3363	592.84	-	9.7754	0.9728

Table 6. Thermodynamic parameters and their values

T (K)	$\Delta G°$ (kJ mol^{-1})	K_{eq}	$\Delta H°$ kJ mol^{-1})	$\Delta S°$ (J mol^{-1}K^{-1})
298	-10.9	81.4	-27.2	-54.7
318	-9.8	40.7		
328	-9.3	30.3		

Table 7. Comparison of BR46 removal using different raw adsorbents

Raw adsorbent	Q_{max} (mg g^{-1})	Reference
Almond skin	57.45	(Atmani et al., 2024)
Coconut shells	68.52	(Jóźwiak et al., 2018)
Olive pomace	14.15	(Graba et al., 2022)
Princess tree leaf	43.10	(Deniz et al., 2011)
Raw Cactus fruit peels	82.58	(Akkari et al., 2023)
Raw Pomegranate peels	86.13	(Akkari et al., 2024)
Raw corn cob	34.95	This study

Negative values of $\Delta G°$ were obtained, -10.9 kJ mol^{-1}, -9.8 kJ mol^{-1} and -9.3 kJ mol^{-1} at 298, 318, and 328 K respectively, which reflect the spontaneity and feasibility of the process. A slight decrease in its value with increasing temperature suggests that the process preferably takes places at low temperatures, which is favorable for the purpose of scaling-up. For the enthalpy change (ΔH^0) a negative value of -27.2 kJ mol^{-1} was found, indicating that the process is exothermic. Finally, the change in entropy (ΔS^0) was -54.7 J mol^{-1} K^{-1}. This negative value can be explained by the loss of degrees of freedom in the movement of the molecules that, when adsorbed, experience a significant decrease in their vibration capacity (Lu et al., 2005; Saha et al., 2011). Furthermore, a negative entropy change suggests the formation of a complex between the adsorbate and the adsorbent, without significant changes in the structure of the adsorbent during adsorption (Saha et al., 2011).

Finally, Table 7 shows the maximum removal load for some raw adsorbents used for RB46 removal, which was obtained under the best removal conditions of each research project. The disparity in this uptake capacity is probably associated with the nature of each adsorbent material, that is, with its bromatological composition, and with the best conditions found for the effectiveness of the adsorption process. In this research, a maximum removal load of 34.95 mg g^{-1} was obtained for raw CC, which is quite satisfactory given the minimum cost of this agricultural by-product and its great abundance in our country, so that its implementation as an adsorbent material in a future scaling process would allow its real valorization as a by-product, contributing significantly to a green process for environmental improvement.

CONCLUSIONS

The current work assessed the sorption ability of corn cob as an alternative, eco-friendly, and inexpensive adsorbent for removing the BR46 dye using statistical tools to obtain a more accurate and reproducible model with greater efficiency. In this way, initially a 2^3 full factorial design with a central point allowed to evaluate the influencing factors on the adsorption process of BR46, finding that the adsorbent dosage was the most important factor, followed by the initial dye concentration and the contact time. Regarding the interactions, a statistically significant and positive effect was observed between dosage and initial dye concentration. Subsequently, with the information provided by the statistical narrowing design, the best conditions for the BR46 removal were identified as a dosage of 5.0 g L^{-1}, an initial BR46 concentration of 15.2 mg L^{-1}, and a contact time of 201.3 minutes, achieving an adsorption efficiency of 97.3%. Finally, process optimization through a central composite response surface design, enabled the identification of the maximum removal point, which reached 98.1%, under the following conditions, a dosage of 5.5 g L^{-1}, an initial concentration of BR46 of 16.6 mg L^{-1}, and contact time of 201.9 minutes.

Under the optimized removal conditions of BR46, it was found that the kinetics of the process present a better fit with the pseudo-second-order model; regarding equilibrium, a good adjustment was observed with the Redlich-Peterson and Langmuir-Freundlich isotherms, with an average correlation coefficient $R^2 = 0.997$ and $R^2 = 0.996$ respectively. Concerning the thermodynamic characteristics of the process, its spontaneous and exothermic nature was confirmed with negative values for the Gibbs free energy and enthalpy, while the negative entropy indicated a decrease in molecular vibrations by the molecules adsorbed at the interface. All these results are highly favorable in the future perspective of carrying this removal process on a larger scale. Furthermore, this research demonstrated the improvement in water quality after the adsorption process, as evidenced by a 29% reduction in COD. This result highlights not only the effectiveness of the adsorption methodology, but also the relevance of COD as an adequate, efficient, and accessible parameter for estimating water quality improvement.

Acknowledgments

The authors express their gratitude to the Universidad Nacional de Colombia Sede Medellín for the financial support through Project code 57756, as well as for the infrastructure of the Experimental Chemistry Laboratory.

REFERENCES

1. Abrile MG, Fiasconaro ML, Lovato ME (2020) Optimization of Reactive Blue 19 dye removal using ozone and ozone/UV employing response surface methodology. *SN Appl Sci 2*:995. https://doi.org/10.1007/s42452-020-2824-y
2. Aigbe UO, Ukhurebor KE, Onyancha RB, Osibote OA, Darmokoesoemo H, Kusuma HS (2021) Fly ash-based adsorbent for adsorption of heavy metals and dyes from aqueous solution: a review. *J Mater Res Technol 14*:2751–2774. https://doi.org/10.1016/j.jmrt.2021.07.140
3. Akkari I, Graba Z, Bezzi N, Merzeg FA, Bait N, Ferhati A (2023) Raw pomegranate peel as promise efficient biosorbent for the removal of Basic Red 46 dye: equilibrium, kinetic, and thermodynamic studies. *Biomass Convers Biorefin 13*:8047–8060. https://doi.org/10.1007/s13399-021-01620-9
4. Akkari I, Graba Z, Bezzi N, Merzeg FA, Bait N, Ferhati A, Kaci MM (2024) Biosorption of Basic Red 46 using raw cactus fruit peels: equilibrium, kinetic and thermodynamic studies. *Biomass Convers Biorefin 14*:1825–1836. https://doi.org/10.1007/s13399-022-02354-y
5. Akter M, Rahman FBA, Abedin MZ, Kabir SMF (2021) Adsorption characteristics of banana peel in the removal of dyes from textile effluent. *Text 1*:361–375. https://doi.org/10.3390/textiles1020018
6. Aldemir A, Turan A, Kul AR, Koyuncu H (2023) Comprehensive investigation of Basic Red 46 removal by pinecone adsorbent: experimental, isotherm, kinetic and thermodynamic studies. *Int J Environ Sci Technol 20*:2601–2622. https://doi.org/10.1007/s13762-022-04456-6
7. Al-Ghouti MA, Da'ana DA (2020) Guidelines for the use and interpretation of adsorption isotherm models: A review. *J Hazard Mater 393*:122383. https://doi.org/10.1016/j.jhazmat.2020.122383
8. Al-Tohamy, R., Ali, S. S., Li, F., Okasha, K. M., Mahmoud, Y. A., Elsamahy, T., Jiao, H., Fu, Y., Sun, J. (2022). A critical review on the treatment of dye-containing wastewater: Ecotoxicological and health concerns of textile dyes and possible remediation approaches for environmental safety. *Ecotoxicology and environmental safety*, *231*:113160. https://doi.org/10.1016/j.ecoenv.2021.113160
9. Aqeel K, Mubarak HA, Amoako-Attah J, Abdul-Rahaim LA, Al Khaddar R, Abdellatif M, … Hashim KS (2020) Electrochemical removal of brilliant green dye from wastewater. *IOP Conf Ser Mater Sci Eng 888*:012036. https://doi.org/10.1088/1757-899X/888/1/012036
10. Área metropolitana Valle de Aburrá (2019) – (in Spanish). Aunar esfuerzos para la gestión integral del recurso hídrico superficial y subterráneo. https://www.metropol.gov.co/ambiental/recurso-hidrico/ResumenesEje/7.%20Resumen-Ejecutivo-Convenio%20643%20de%202019%20V1.pdf (Accessed 19 Jan 2025).
11. Atkins P, de Paula JD (2022) *Atkins' Physical Chemistry, 8th edn.*
12. Atmani F, Balamane-Zizi O, Akkari I et al (2024) The potential of almond skin as a sustainable biomaterial for eliminating azo dye in aqueous media. *Water Air Soil Pollut 235*:257. https://doi.org/10.1007/s11270-024-07057-w
13. Bushra R, Mohamad S, Alias Y, Jin Y, Ahmad M (2021) Current approaches and methodologies to explore the perceptive adsorption mechanism of dyes on low-cost agricultural waste: A review. *Microporous Mesoporous Mater 319*:111040. https://doi.org/10.1016/j.micromeso.2021.111040
14. Castro AM, Nogueira V, Lopes I, Rocha-Santos T, Pereira R. (2019). Evaluation of the Potential Toxicity of Effluents from the Textile Industry before and after Treatment. *Applied Sciences*, *9*(18), 3804. https://doi.org/10.3390/app9183804

15. Chen T, Da T, Ma Y (2021) Reasonable calculation of the thermodynamic parameters from adsorption equilibrium constant. *J Mol Liq 322*:114980. https://doi.org/10.1016/j.molliq.2020.114980.
16. Crini G (2006) Non-conventional low-cost adsorbents for dye removal: A review. *Bioresour Technol 97*:1061–1085. https://doi.org/10.1016/j.biortech.2005.05.001
17. Cueva-Orjuela JC, Hormaza-Anaguano A, Merino-Restrepo A (2017) Sugarcane bagasse and its potential use for the textile effluent treatment. *Dyna (Medellin) 84*:291–297. https://doi.org/10.15446/dyna.v84n203.61723
18. Dada AO, Olalekan A, Olatunya A, Dada O (2012) Langmuir, Freundlich, Temkin and Dubinin–radushkevich isotherms studies of equilibrium sorption of Zn^{2+} unto phosphoric acid modified rice husk. *J Appl Chem 3*:38–45. https://doi.org/10.9790/5736-0313845
19. Deniz F, Saygideger SD (2011) Removal of a hazardous azo dye (Basic Red 46) from aqueous solution by princess tree leaf. *Desalination 268*:6–11. https://doi.org/10.1016/j.desal.2010.09.043
20. Echavarria-Alvarez AM, Hormaza-Anaguano A (2014) Flower wastes as a low-cost adsorbent for the removal of acid blue 9. *Dyna (Medellin) 81*:131–137. https://www.redalyc.org/articulo.oa?id=49631031019 (Accessed 05 Jun 2024)
21. Fan M, Dai D, Huang B (2012) Fourier transform infrared spectroscopy for natural fibres. In: *Fourier Transform – Materials Analysis,* 45–68. https://doi.org/10.5772/35482
22. FAO (2009) How to feed the world in 2050. https://www.fao.org/fileadmin/templates/wsfs/docs/expert_paper/How_to_Feed_the_World_in_2050.pdf (Accessed 05 Jun 2024)
23. Graba Z, Akkari I, Bezzi N, Kaci MM (2022) Valorization of olive–pomace as a green sorbent to remove Basic Red 46 (BR46) dye from aqueous solution. *Biomass Convers Biorefin.* https://doi.org/10.1007/s13399-022-03639-y.
24. Gupta VK, Suhas (2009) Application of low-cost adsorbents for dye removal – A review. *J Environ Manage 90*: 2313–2342. https://doi.org/10.1016/j.jenvman.2008.11.017
25. Hameed BH, Tan IAW, Ahmad AL (2008) Adsorption isotherm, kinetic modeling and mechanism of 2,4,6-trichlorophenol on coconut husk-based activated carbon. *Chem Eng J 144*:235–244. https://doi.org/10.1016/J.CEJ.2008.01.028
26. Ihaddaden S, Aberkane D, Boukerroui A, Robert D (2022) Removal of methylene blue (basic dye) by coagulation-flocculation with biomaterials. *J Water Process Eng 49*:102952. https://doi.org/10.1016/j.jwpe.2022.102952
27. ISO (2002) ISO 15705:2002 Water quality — Determination of the chemical oxygen demand index (ST-COD) — Small-scale sealed-tube method. EDITION 1. https://www.iso.org/standard/28778.html (Accessed 25 Jan 2025)
28. Jabar JM, Odusote YA, Ayinde YT, Yılmaz M (2022) African almond (*Terminalia catappa* L) leaves biochar prepared through pyrolysis using H_3PO_4 as chemical activator for sequestration of methylene blue dye. *Results Eng 14*:100385. https://doi.org/10.1016/j.rineng.2022.100385
29. Jóźwiak T, Filipkowska U, Bugajska P, Kalkowski T (2018) The use of coconut shells for the removal of dyes from aqueous solutions. *J Ecol Eng 19*:129–135. https://doi.org/10.12911/22998993/89672
30. Jóźwiak T, Filipkowska U, Marciniak P (2021) Use of hen feathers to remove Reactive Black 5 and Basic Red 46 from aqueous solutions. *Desalination Water Treat 232*:129–139. https://doi.org/10.5004/dwt.2021.27513
31. Kaouah F, Boumaza S, Berrama T, Trari M, Bendjama Z (2013) Preparation and characterization of activated carbon from wild olive cores (oleaster) by H_3PO_4 for the removal of Basic Red 46. *J Clean Prod 54*:296–306. https://doi.org/10.1016/j.jclepro.2013.04.038
32. Kiani Ghaleh Sardi F, Behpour M, Ramezani Z, Masoum S (2021) Simultaneous removal of Basic Blue 41 and Basic Red 46 dyes in binary aqueous systems via activated carbon from palm bio-waste. *Environ Technol Innov 24*:102039. https://doi.org/10.1016/j.eti.2021.102039
33. Kowalski SM, Borror CM, Montgomery DC (2005) A modified path of steepest ascent for split-plot experiments. *J Qual Technol 37*:75–83. https://doi.org/10.1080/00224065.2005.11980302
34. Langmuir I (1916) The evaporation; condensation and reflection of molecules and the mechanism of adsorption. *Phys Rev 8*:149–176. https://doi.org/10.1103/PhysRev.8.149
35. Li, T., Wei, L., Fang, Y., Cui, Y., Wang, X., Li, Y. (2025). Risk identification of human health, ecotoxicity, and degradation products of azo dyes: development of a priority control list. *Environmental pollution*, *386*, 127180. Advance online publication. https://doi.org/10.1016/j.envpol.2025.127180
36. Lu B, Wong CF (2005) Direct estimation of entropy loss due to reduced translational and rotational motions upon molecular binding. *Biopolym 79*:277–285. https://doi.org/10.1002/bip.20344
37. Mañunga T, Gutiérrez HM, Rodríguez JA, Villareal A (2010) (in Spanish) Tratamiento de residuos de DQO generados en laboratorios de análisis ambientales. *Ing Investig 30*:87–95. https://www.redalyc.org/articulo.oa?id=64316114009 (Accessed 25 Apr 2024)

38. Ministerio de Agricultura y Desarrollo Rural (2021) (in Spanish) Maíz. https://sioc.minagricultura.gov.co/AlimentosBalanceados/Documentos/2021-03-31%20Cifras%20Sectoriales%20ma%C3%ADz.pdf (Accessed 05 Jun 2024)
39. Ministerio de ambiente y desarrollo sostenible (2015) (in Spanish) Resolución 631 de 2015. https://www.minambiente.gov.co/wp-content/uploads/2021/11/resolucion-631-de-2015.pdf (Accessed 26 Jul 2024)
40. Pavithra KG, Kumar PS, Jaikumar V, Rajan PS (2019) Removal of colorants from wastewater: A review on sources and treatment strategies. *J Ind Eng Chem 75*:1–19. https://doi.org/10.1016/j.jiec.2019.02.011
41. Pereira L, Alves M (2012) *Dyes—Environmental Impact and Remediation*. In: Environ. Protection Strategies for Sustain. Dev. Dordrecht: Springer Netherlands, pp 111–162. https://doi.org/10.1007/978-94-007-1591-2_4
42. Pérez-Marín AB, Zapata VM, Ortuño JF, Aguilar M, Sáez J, Lloréns M (2007) Removal of cadmium from aqueous solutions by adsorption onto orange waste. *J Hazard Mater 139*:122–131. https://doi.org/10.1016/j.jhazmat.2006.06.008
43. Robinson T, McMullan G, Marchant R, Nigam P (2001) Remediation of dyes in textile effluent: a critical review on current treatment technologies with a proposed alternative. *Bioresour Technol 77*:247–255. https://doi.org/10.1016/S0960-8524(00)00080-8
44. Saeed M, Muneer M, Haq A, Akram N (2022) Photocatalysis: an effective tool for photodegradation of dyes – a review. *Environ Sci Pollut Res 29*:293–311. https://doi.org/10.1007/s11356-021-16389-7
45. 45. Saha P, Chowdhury S (2011) Insight into adsorption thermodynamics. In: *Thermodyn, 16*:349–364. https://doi.org/10.5772/13474
46. Salgar LM (2005) (in Spanish) El cultivo de maíz en Colombia. https://www.semillas.org.co/es/el-cultivo-de-maz-en-colombia (Accessed 30 May 2024)
47. Shinde RM, Ingle PU, Trivedi HR, Wasule D, Gaharwar A, Gade AK,..., Biswas JK (2024) Bioremediation of industrial dye waste effluents aided by GIS applications: a comprehensive review. *Environ Dev Sustain 26*:10945–10971. https://doi.org/10.1007/s10668-023-03722-y
48. Smith BC (2018) Infrared spectral interpretation: A systematic approach. https://doi.org/10.1201/9780203750841
49. Srinivasan A, Viraraghavan T (2010) Decolorization of dye wastewaters by biosorbents: A review. *J Environ Manage 91*:1915–1929. https://doi.org/10.1016/j.jenvman.2010.05.003
50. Supelco (2020) COD solutions A+B. https://www.sigmaaldrich.com/deepweb/assets/sigmaaldrich/product/documents/133/441/cod-solutions-a-b-su06-en.pdf (Accessed 31 May 2024)
51. Tran HN, Lima EC, Juang R-S, Bollinger J-C, Chao H-P (2021) Thermodynamic parameters of liquid–phase adsorption process calculated from different equilibrium constants related to adsorption isotherms: A comparison study. *J Environ Chem Eng 9*:106674. https://doi.org/10.1016/j.jece.2021.106674
52. Trivizadakis ME, Giakoumakis D, Karabelas AJ (2006) A study of particle shape and size effects on hydrodynamic parameters of trickle beds. *Chem Eng Sci 61*. https://doi.org/10.1016/j.ces.2006.03.025
53. Velandia-Ciendua M, Hormaza A (2019) Utilización del método alternativo con azul de metileno para la estimación del área superficial específica de un adsorbente (in Spanish). Libro de Resúm. del XXI Congreso Argent. de Investig. Fisicoquím. y Quím. Inorg, p. 221.
54. Wang J, Guo X (2020a) Adsorption kinetic models: Physical meanings, applications, and solving methods. *J Hazard Mater 390*:122156. https://doi.org/10.1016/j.jhazmat.2020.122156
55. Wang J, Guo X (2020b) Adsorption isotherm models: Classification, physical meaning, application and solving method. *Chemosphere 258*:127279. https://doi.org/10.1016/j.chemosphere.2020.127279
56. Wang J, Hu X (2021) Research on corn production efficiency and influencing factors of typical farms: Based on data from 12 corn-producing countries from 2012 to 2019. *PLoS One 16*. https://doi.org/10.1371/journal.pone.0254423
57. Yadav, M., Singh, N., Annu, Khan, S. A., Raorane, C. J., Shin, D. K.. (2024). Recent advances in utilizing lignocellulosic biomass materials as adsorbents for textile dye removal: A comprehensive review. *Polymers, 16*(17), 2417. https://doi.org/10.3390/polym1617241
58. Zheng L, Dang Z, Yi X, Zhang H (2010) Equilibrium and kinetic studies of adsorption of Cd (II) from aqueous solution using modified corn stalk. *J Hazard Mater 176*(1–3):650–656. https://doi.org/10.1016/j.jhazmat.2009.11.081
59. Zuluaga Díaz B, Hormaza Anaguano A, Beltrán Pérez ÓD, Cardona Gallo SA (2014) Statistical design for the removal of basic red 46 using regenerated fuller earth as an alternative material. *Rev EIA 11*. https://revistabme.eia.edu.co/index.php/Reveiaenglish/article/view/943 (Accessed 19 Jan 2025)